Inorg. Chem. **2005**, *44*, 9567–9573

New Linear High-Valent Tetranuclear Manganese-Oxo Cluster Relevant to the Oxygen-Evolving Complex of Photosystem II with Oxo, Hydroxo, and Aqua Coordinated to a Single Mn(IV)

Hongyu Chen,[†,#] Marie-Noëlle Collomb,[‡] Carole Duboc,[§] Geneviève Blondin,[||] Eric Rivière,[||] J. W. Faller,[†] Robert H. Crabtree,*[,†] and Gary W. Brudvig*[,†]

Department of Chemistry, Yale University, P.O. Box 208107, New Haven, Connecticut 06520-8107, Laboratoire d'Electrochimie Organique et de Photochimie Rédox, UMR CNRS 5630, Université Joseph Fourier and Institut de Chimie Moléculaire de Grenoble, FR CNRS 2607, BP 53, 38041 Grenoble Cedex 9, France, Grenoble High Magnetic Field Laboratory, Laboratoire des Champs Magnétiques Intenses, CNRS UPR 5021, MPI BP 166, 38042 Grenoble Cedex 9, France, and Laboratoire de Chimie Inorganique, UMR CNRS 8613, Institut de Chimie Moléculaire et des Matériaux d'Orsay, Université Paris-Sud, 91405 Orsay Cedex, France

Received August 26, 2005

An unprecedented atom connectivity, $Mn^{IV}(\mu\text{-}O)Mn^{IV}(\mu\text{-}O)_2Mn^{IV}(\mu\text{-}O)Mn^{IV}$, is found in the complex $[Mn^{IV}_4O_4(EtO\text{-}terpy)_4(OH)_2(OH_2)_2](ClO_4)_6\cdot 8H_2O$ (EtO-terpy = 4′-ethoxyl-2,2′:6′,2″-terpyridine), which has been characterized by X-ray crystallography, X-ray powder diffraction, EPR spectroscopy, and magnetic studies. This complex is the first example of a compound where a Mn^{IV} ion is coordinated by all three types of water-derived ligands: oxo, hydroxo, and aqua. Bond distances and angles for this complex are consistent with a Mn^{IV}_4 oxidation state assignment. The di-μ-oxo- and mono-μ-oxo-bridged Mn–Mn distances are 2.80 and 3.51 Å, respectively. The variable-temperature magnetic susceptibility data for this complex, in the range of 10–300 K, are consistent with an $S = 0$ ground state and were fit using the spin Hamiltonian $\hat{H}_{HDvV} = -J_1\hat{S}_2\hat{S}_1 - J_2\hat{S}_1\hat{S}_{1A} - J_1\hat{S}_{1A}\hat{S}_{2A}$ ($S_1 = S_{1A} = S_2 = S_{2A} = 3/2$) with $J_1 = -432$ cm^{-1} and $J_2 = -164$ cm^{-1} (where J_1 and J_2 are exchange constants through the mono-μ-oxo and the di-μ-oxo bridges, respectively). The first excited spin state of this tetramer is a spin triplet state at 279 cm^{-1} above the diamagnetic ground state. The next spin states are the $S = 1$ and $S = 2$ levels at about 700 and 820 cm^{-1} above the $S = 0$ ground state, respectively. These large energy gaps are consistent with the absence of an EPR signal for this complex, even at high temperature.

Introduction

The oxidation of water to molecular oxygen is one of the most important and fundamental biological processes in nature. This reaction, carried out on a global scale in green plants and cyanobacteria, is known to be catalyzed by a tetranuclear manganese cluster in the oxygen-evolving complex (OEC) of photosystem II (PS II). X-ray absorption spectroscopic (XAS) studies have provided evidence for the existence of Mn−(μ-O)$_2$−Mn and Mn−(μ-O)−Mn moieties in the Mn tetramer,[1] while the recent EPR/ENDOR studies[2,3] and crystal structures (3.8, 3.7, and most recently, 3.5 Å resolution) of PS II suggested that the four Mn ions of the OEC are organized in a "3 + 1" fashion,[4,5] possibly as a $CaMn_3O_4$ cubane linked to a fourth Mn.[6] However, at the current resolution, the ligands of the Mn tetramer, particularly

* To whom correspondence should be addressed. E-mail: gary.brudvig@yale.edu (G.W.B.); robert.crabtree@yale.edu (R.H.C.).
† Yale University.
# Current Address: Department of Food Science, Cornell University.
‡ Laboratoire d'Electrochimie Organique et de Photochimie Rédox.
§ High Magnetic Field Laboratory.
|| Laboratoire de Chimie Inorganique.

(1) Yachandra, V. K.; Sauer, K.; Klein, M. P. *Chem. Rev.* **1996**, *96*, 2927.
(2) Peloquin, J. M.; Campbell, K. A.; Randall, D. W.; Evanchik, M. A.; Pecoraro, V. L.; Armstrong, W. H.; Britt, R. D. *J. Am. Chem. Soc.* **2000**, *122*, 10926.
(3) Britt, R. D.; Peloquin, J. M.; Campbell, K. A. *Annu. Rev. Biophys. Biomolec. Struct.* **2000**, *29*, 463.
(4) Zouni, A.; Witt, H. T.; Kern, J.; Fromme, P.; Krauss, N.; Saenger, W.; Orth, P. *Nature* **2001**, *409*, 739.
(5) Kamiya, N.; Shen, J. R. *Proc. Natl. Acad. Sci. U.S.A.* **2003**, *100*, 98.
(6) Ferreira, K. N.; Iverson, T. M.; Maghlaoui, K.; Barber, J.; Iwata, S. *Science* **2004**, 1.

10.1021/ic051462m CCC: $30.25
Published on Web 10/25/2005

Scheme 1. Oxo−Manganese Core Structures of Known High-Valent Manganese Tetramers

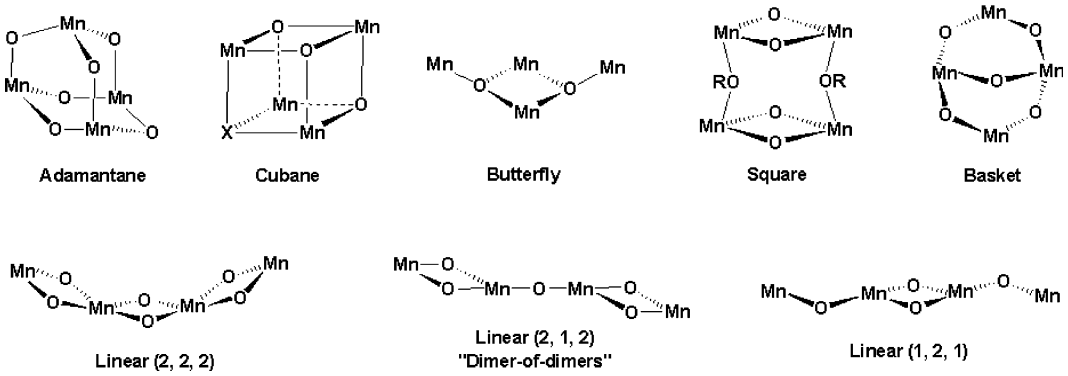

the small ligands such as oxo, hydroxo, chloride, water, and carbonate, cannot be confidently assigned.

Studies of inorganic Mn complexes have provided insights for the chemical and physical properties of the Mn tetramer in the OEC,[7] such as IR/Raman frequencies of Mn-related resonances,[8] Mn−ligand bond distances and Mn−Mn separations,[1,9] magnetic properties of Mn clusters, and the general coordination environments of high-valent Mn species. For these purposes, high-valent manganese tetramer complexes are of particular interest as structural models for the OEC. The complexes known in the literature can be divided into six classes according to the atom connectivity of their Mn_4O_x core: (a) butterfly,[10−14] (b) square,[15] (c) adamantane,[16−18] (d) cubane,[19−24] (e) basket,[25] and (f) linear[26−28] (Scheme 1). So far, there are only two linear Mn tetramer complexes. Girerd and co-workers synthesized $[Mn^{IV}_4O_6(bpy)_6]^{4+}$ (**1**)[26,27] (bpy = 2,2′-bipyridine) with each of the Mn ions linked to an adjacent Mn^{IV} ion via a di-μ-oxo bridge, $Mn(\mu\text{-}O)_2Mn$-$(\mu\text{-}O)_2Mn(\mu\text{-}O)_2Mn$. In this report, we identify this structural type as "linear (2, 2, 2)" to specify the number of oxo ligands between the Mn ions. Recently, we reported the first "dimer-of-dimers" model complex, $[Mn^{IV}_4O_5(terpy)_4(OH_2)_2]^{6+}$ (**2**)[28] (terpy = 2,2′:6′,2″-terpyridine), where a pair of Mn−di-μ-oxo−Mn units are connected via a mono-μ-oxo bridge (linear (2, 1, 2)). This type of Mn−oxo core structure has been a leading candidate for the structure of the Mn tetramer in the OEC,[1,29] although the recent EPR/ENDOR studies[2,3] and PS II crystal structures[4−6] favor a 3 + 1 model (vide supra). Complex **2** is one of only a few examples of high-valent oxomanganese tetramers with coordinated waters.[10,11,30] Such complexes are of particular interest because water is the substrate of the OEC.

Here, we report the synthesis, crystal structure, and magnetic properties of $[Mn^{IV}_4O_4(EtO\text{-}terpy)_4(OH)_2(OH_2)_2](ClO_4)_6$ (**3**, EtO-terpy = 4′-ethoxy-2,2′:6′,2″-terpyridine), where a di-μ-oxo bridge links a pair of Mn−mono-μ-oxo−Mn units to form a new linear core (linear (1, 2, 1), Scheme 1). The di-μ-oxo- and mono-μ-oxo-bridged Mn−Mn distances are 2.80 and 3.51 Å, respectively. This complex is also the first example, to our knowledge, of a compound where all three types of water-derived ligands, oxo, hydroxo, and aqua, coordinate to a Mn^{IV} ion. Such coordination of aqua ligands previously has only been found in a Mn^{III}-substituted tungstosilicate, $[(SiO_4)W_{10}Mn^{III}_2O_{36}H_6]^{4-}$,[31] where stable tungstate provides oxo-coordination to Mn^{III} ions, and in several other cases for heavy elements such as Mo,[32,33] Nb,[34] W,[35,36] and U.[37] Complex **3** provides structural evidence

(7) Mukhopadhyay, S.; Mandal, S. K.; Bhaduri, S.; Armstrong, W. H. *Chem. Rev.* **2004**, *104*, 3981.
(8) Chu, H. A.; Hillier, W.; Law, N. A.; Babcock, G. T. *Biochim. Biophys. Acta* **2001**, *1503*, 69.
(9) Manchanda, R.; Brudvig, G. W.; Crabtree, R. H. *Coord. Chem. Rev.* **1995**, *144*, 1.
(10) Wang, S. Y.; Huffman, J. C.; Folting, K.; Streib, W. E.; Lobkovsky, E. B.; Christou, G. *Angew. Chem., Int. Ed. Engl.* **1991**, *30*, 1672.
(11) Wemple, M. W.; Tsai, H. L.; Wang, S. Y.; Claude, J. P.; Streib, W. E.; Huffman, J. C.; Hendrickson, D. N.; Christou, G. *Inorg. Chem.* **1996**, *35*, 6437.
(12) (a) Vincent, J. B.; Christmas, C.; Huffman, J. C.; Christou, G.; Chang, H. R.; Hendrickson, D. N. *J. Chem. Soc., Chem. Commun.* **1987**, 236. (b) Vincent, J. B.; Christmas, C.; Chang, H. R.; Li, Q. Y.; Boyd, P. D. W.; Huffman, J. C.; Hendrickson, D. N.; Christou, G. *J. Am. Chem. Soc.* **1989**, *111*, 2086.
(13) Kulawiec, R. J.; Crabtree, R. H.; Brudvig, G. W.; Gayle, K.; Schulte, G. K. *Inorg. Chem.* **1988**, *27*, 1309.
(14) Vincent, J. B.; Chang, H. R.; Folting, K.; Huffman, J. C.; Christou, G.; Hendrickson, D. N. *J. Am. Chem. Soc.* **1987**, *109*, 5703.
(15) Chan, M. K.; Armstrong, W. H. *J. Am. Chem. Soc.* **1991**, *113*, 5055.
(16) Dube, C. E.; Wright, D. W.; Pal, S.; Bonitatebus, P. J.; Armstrong, W. H. *J. Am. Chem. Soc.* **1998**, *120*, 3704.
(17) Wieghardt, K.; Bossek, U.; Nuber, B.; Weiss, J.; Bonvoisin, J.; Corbella, M.; Vitols, S. E.; Girerd, J. J. *J. Am. Chem. Soc.* **1988**, *110*, 7398.
(18) Hagen, K. S.; Westmoreland, T. D.; Scott, M. J.; Armstrong, W. H. *J. Am. Chem. Soc.* **1989**, *111*, 1907.
(19) Wang, S.; Tsai, H. L.; Streib, W. E.; Christou, G.; Hendrickson, D. N. *J. Chem. Soc., Chem. Commun.* **1992**, 1427.
(20) Wang, S. Y.; Tsai, H. L.; Hagen, K. S.; Hendrickson, D. N.; Christou, G. *J. Am. Chem. Soc.* **1994**, *116*, 8376.
(21) Ruettinger, W. F.; Campana, C.; Dismukes, G. C. *J. Am. Chem. Soc.* **1997**, *119*, 6670.
(22) Gedye, C.; Harding, C.; McKee, V.; Nelson, J.; Patterson, J. *J. Chem. Soc., Chem. Commun.* **1992**, 392.
(23) Wang, S. Y.; Folting, K.; Streib, W. E.; Schmitt, E. A.; McCusker, J. K.; Hendrickson, D. N.; Christou, G. *Angew. Chem., Int. Ed. Engl.* **1991**, *30*, 305.
(24) Bashkin, J. S.; Chang, H. R.; Streib, W. E.; Huffman, J. C.; Hendrickson, D. N.; Christou, G. *J. Am. Chem. Soc.* **1987**, *109*, 6502.
(25) Mukhopadhyay, S.; Staples, R. J.; Armstrong, W. H. *J. Chem. Soc., Chem. Commun.* **2002**, 864.
(26) Philouze, C.; Blondin, G.; Girerd, J. J.; Guilhem, J.; Pascard, C.; Lexa, D. *J. Am. Chem. Soc.* **1994**, *116*, 8557.
(27) Philouze, C.; Blondin, G.; Menage, S.; Auger, N.; Girerd, J. J.; Vigner, D.; Lance, M.; Nierlich, M. *Angew. Chem., Int. Ed. Engl.* **1992**, *31*, 1629.
(28) Chen, H. Y.; Faller, J. W.; Crabtree, R. H.; Brudvig, G. W. *J. Am. Chem. Soc.* **2004**, *126*, 7345.
(29) Yachandra, V. K.; DeRose, V. J.; Latimer, M. J.; Mukerji, I.; Sauer, K.; Klein, M. P. *Science* **1993**, *260*, 675.
(30) Suzuki, M.; Hayashi, Y.; Munezawa, K.; Suenaga, M.; Senda, H.; Uehara, A. *Chem. Lett.* **1991**, 1929.
(31) Zhang, X. Y.; O'Connor, C. J.; Jameson, G. B.; Pope, M. T. *Inorg. Chem.* **1996**, *35*, 30.

for the sequential deprotonated states of aqua ligands on a high-valent oxo-manganese(IV) complex.

Experimental Section

All solutions were prepared using doubly deionized water. EtO-terpy was synthesized following previous procedures.[38] Oxone ($2KHSO_5 \cdot KHSO_4 \cdot K_2SO_4$) was purchased from Acros Organics and was standardized using iodometric titrations. All other chemicals were purchased from Aldrich and used without further purification. NMR spectra were recorded on Bruker DPX 400 and 500 MHz instruments. Elemental analyses were performed by Atlantic Microlabs Inc., Norcross, GA.

Synthesis of $[Mn^{IV}_4O_4(EtO\text{-}terpy)_4(OH)_2(OH_2)_2](ClO_4)_6$ (3). EtO-terpy (0.146 g, 0.525 mmol, 1.05 equiv) was dissolved in CH_3CN (125 mL), to which $MnCl_2 \cdot 10H_2O$ (0.099 g, 0.5 mmol, 1 equiv) in H_2O (100 mL) was added. After all reactants were dissolved, the yellow mixture was stirred in an ice bath for 10 min. Oxone (0.134 g, 2.79 mmol $KHSO_5$ per g, 0.375 mmol, 0.75 equiv) in H_2O (25 mL) was then added to the mixture, which turned deep green in about 5 min. A large excess of solid $NaClO_4 \cdot H_2O$ (16 g) was added to the mixture, and the pH of the solution was adjusted to 2 by the addition of concentrated HNO_3. ***CAUTION:*** *Perchlorates and their solutions are potentially explosive; even though no accident occurred during handling, extreme caution should be used.* The resulting red solution was transferred to a series of test tubes and allowed to slowly evaporate in the dark. Black-red plate crystals of $\mathbf{3} \cdot 8H_2O$ formed in about two weeks, with the supernatant now turned to a light brown color. The crystals were filtered off and washed first with CH_3CN (5×1 mL) and then with copious amounts of diethyl ether. Drying under vacuum overnight gives the octahydrate complex (0.145 g, 70% yield based on oxone). Anal. Calcd for $C_{68}H_{66}Cl_6Mn_4N_{12}O_{36} \cdot 8H_2O$: C, 37.04; H, 3.75; N, 7.63. Found: C, 36.85; H, 3.47; N, 7.73. IR (KBr, cm^{-1}): 3452(s, br), 3085(m, br), 1615(s), 1558(m), 1481(s), 1445(m), 1432(m), 1400(w), 1380(m), 1361(m), 1254(w), 1226(s), 1167(m), 1097(s, br), 1035(s), 840(m), 788(m), 700(m), 677(m), 661(m), 624(s).

Crystal Structure Determination of 3. A dark red plate crystal of $\mathbf{3} \cdot 8H_2O$ with approximate dimensions of $0.10 \times 0.12 \times 0.19$ mm was mounted on a fiber. All measurements were made on a Nonius KappaCCD diffractometer with graphite monochromated Mo Kα ($\lambda = 0.71069$ Å) radiation. The crystallographic data are summarized in Table 1. The structure was solved by direct methods and expanded using Fourier techniques. The non-hydrogen atoms not involved in disorders were refined anisotropically. Hydrogen atoms that could not be located on the aqua ligands or on the lattice water molecules were ignored in the refinement. Other hydrogen atoms were included in calculated positions. The investigation of voids using Platon[39] (with and without the disordered perchlorates and larger amplitude water oxygen atoms) indicated the presence of a total number of uncoordinated waters in the asymmetric unit of $\sim 6-7$. SQUEEZE[39] corrections for disordered solvent did not give satisfactory results. The final cycle of full-matrix least-squares refinement on F was based on 4109 observed reflections ($I > 3.00\sigma(I)$) and 631 variable parameters and converged with unweighted and weighted agreement factors of $R = 0.072$ and $R_w = 0.074$. On the basis of an occupancy of eight uncoordinated water molecules per tetrameric unit, the formula weight was determined to be 2203.92 which gives a calculated density of 1.63 g/cm^3. Oxygen atoms of uncoordinated water molecules were refined at full occupancy, but large thermal parameters for some atoms might reflect partial occupancy and indicate that eight uncoordinated water molecules per tetrameric unit may overestimate the true solvation.

Table 1. X-ray Crystallographic Data for $\mathbf{3} \cdot 8H_2O$

empirical formula	$C_{68}H_{82}Cl_6Mn_4N_{12}O_{44}$
fw	2203.92
cryst syst	monoclinic
space group	*C*2/*c* (No. 15)
a (Å)	28.3800(13)
b (Å)	16.2321(7)
c (Å)	21.2370(9)
β (deg)	119.883(2)
V (Å^3)	8482.4(7)
Z	4
T (°C)	- 90(1)
λ (Å)	0.71069
d_{calcd} (g/cm^3)	1.634
F_{000}	4268.00
reflns collected/unique	17741/10749
no. observations ($I > 3.00\sigma(I)$)	4109
reflns/params	6.51
R,[a] R_w[b]	0.072, 0.074
GOF	2.49

[a] $R = \sum||F_o| - |F_c||/\sum|F_o|$. [b] $R_w = [\sum w(|F_o| - |F_c|)^2/\sum wF_o^2]^{1/2}$.

X-ray Powder diffraction. X-ray powder diffraction (XRD) patterns were recorded at room temperature on a Bruker D8-Focus with Cu Kα ($\lambda = 1.5405$ Å) irradiation. Simulation of the XRD pattern was performed by Mercury 1.3, available from the Cambridge Crystallographic Data Center. No absorption is simulated by the software, and the isotropic atomic displacement parameters (B_{iso}) of the hydrogen and non-hydrogen atoms are assumed to be 6.0 and 3.0, respectively.[40]

EPR Spectroscopy. Perpendicular-mode EPR spectra were collected on an X-band Bruker ESP 300E spectrometer between 100 and 170 K. Low-temperature EPR spectra (from 4 to 77 K) were recorded on a X-band Bruker EMX spectrometer equipped with an Oxford Instruments ESR-900 continuous-flow helium cryostat and an ER-4116 OM Bruker cavity

Magnetic Susceptibility Measurements. Magnetic susceptibility data were recorded on a MPMS5 magnetometer (Quantum Design Inc.). The calibration was made at 298 K using a palladium reference sample furnished by Quantum Design Inc. The data were collected over a temperature range of 10−300 K at a magnetic field of 1000 Oe and were corrected for diamagnetism. The experimental data have been further corrected for the contribution of a mononuclear Mn^{IV} species (0.4%, $S = 3/2$) shown by X-band EPR recordings at helium temperature (data not shown). A Curie law was assumed for this correction.

The van Vleck formula was used to calculate the molar magnetic susceptibility of the tetranuclear complex, assuming a common *g* value for all the spin states. The energy diagram was established using the following Heisenberg−Dirac−van Vleck Hamiltonian

(32) Cadot, E.; Salignac, B.; Marrot, J.; Dolbecq, A.; Secheresse, F. *J. Chem. Soc., Chem. Commun.* **2000**, 261.
(33) Lisnard, L.; Mialane, P.; Dolbecq, A.; Marrot, J.; Secheresse, F. *Inorg. Chem. Commun.* **2003**, *6*, 503.
(34) Galesic, N.; Matkovic, B.; Herceg, M.; Sljukic, M. *J. Less-Common Metals* **1971**, *25*, 234.
(35) Griffith, W. P.; Parkin, B. C.; White, A. J. P.; Williams, D. J. *J. Chem. Soc., Chem. Commun.* **1995**, 2183.
(36) Gresley, N. M.; Griffith, W. P.; White, A. J. P.; Williams, D. J. *J. Chem. Soc., Dalton Trans.* **1997**, 89.
(37) Navaza, A.; Iroulart, M. G.; Navaza, J. *J. Coord. Chem.* **2000**, *51*, 153.
(38) Constable, E. C.; Thompson, A.; Tocher, D. A.; Daniels, M. A. M. *New J. Chem.* **1992**, *16*, 855.
(39) Vandersluis, P.; Spek, A. L. *Acta Crystallogr. A* **1990**, *46*, 194.
(40) Mercury 1.3 User Guide and Tutorials available at http://www.ccdc.cam.ac.uk/support/documentation/mercury/Mercury_Manual.pdf.

$$\hat{H}_{\mathrm{HDvV}} = -J_1\hat{S}_2\,\hat{S}_1 - J_2\hat{S}_1\hat{S}_{1\mathrm{A}} - J_1\hat{S}_{1\mathrm{A}}\hat{S}_{2\mathrm{A}}$$

where the labeling of the spin operators refers to that of the metallic ions in the ORTEP view ($S_1 = S_{1A} = S_2 = S_{2A} = 3/2$), and J_1 and J_2 denote the exchange constants through the mono-μ-oxo and the di-μ-oxo bridges, respectively. Only the total spin, S, is a good quantum number, and the energies were obtained by exact diagonalization of the matrixes associated with each S total spin value.[26]

Results and Discussion

Synthesis of $[Mn^{IV}_4O_4(EtO\text{-}terpy)_4(OH)_2(OH_2)_2](ClO_4)_6\cdot 8H_2O$. The synthesis of $\mathbf{3}\cdot 8H_2O$ is only slightly different from that previously reported for **2**;[28] the replacement of terpy with EtO-terpy led to the isolation of **3** as a deep red crystalline compound. Elemental analysis and XRD results verified that this isolated compound was pure **3** (vide infra). The IR band of **3** at 700 cm^{-1} is typical for compounds with a Mn−di-μ-oxo−Mn core and is comparable to similar bands for **2** (695 cm^{-1}), $[Mn^{III/IV}_2O_2(terpy)_2(OH_2)_2](NO_3)_3$ (**4**, 703 cm^{-1}),[41] and $[Mn^{IV/IV}_2O_2(terpy)_2(SO_4)_2]$ (**5**, 687 cm^{-1}).[42]

X-ray Crystal Structure of 3. As shown in Scheme 1, the oxomanganese core of **3** differs significantly from that of **2**. Instead of the linear (2, 1, 2) core structure of **2**, the two mono-μ-oxo-bridged dimanganese units of **3** are connected via a di-μ-oxo-bridge, forming a linear (1, 2, 1) core structure. The structure of the $[Mn^{IV}_4O_4(EtO\text{-}terpy)_4(OH)_2(OH_2)_2]^{6+}$ cation is represented in Figure 1 (also see Figures S1 and S2 in the Supporting Information). Selected bond distances and angles are listed in Table 2. The cation of **3** possesses a center of inversion, which relates the two Mn−mono-μ-oxo−Mn units. The two EtO-terpy planes of each Mn−mono-μ-oxo−Mn unit are approximately parallel with an interplanar separation of ca. 3.5 Å, suggesting the presence of stacking interactions. The Mn−mono-μ-oxo−Mn distances (3.51 Å) in **3** are exactly the same as those in **2**, while the Mn−di-μ-oxo−Mn distance (2.80 Å) in **3** is slightly longer than that in **2** (2.74 Å).

With six ClO_4^- per Mn tetramer, charge considerations require the assignment of **3** as either $[Mn^{IV/IV/IV/IV}_4O_4(EtO\text{-}terpy)_4(OH)_2(OH_2)_2]^{6+}$ or $[Mn^{III/IV/IV/III}_4O_4(EtO\text{-}terpy)_4(OH_2)_4]^{6+}$. Jahn−Teller effects are expected to distort the coordination geometry of the Mn^{III} (d^4) ions but not the Mn^{IV} (d^3) ions. An elongation of the $Mn^{III}-N_{distal}$ bond was observed in the previously characterized $[Mn^{III/IV}_2O_2(terpy)_2(CF_3CO_2)_2](ClO_4)$ (**6**)[43] and $[Mn^{III/IV}_2O_2(mesityl\text{-}terpy)_2(OH_2)_2](NO_3)_3$ (**7**, mesityl-terpy = 4′-mesityl-2,2′:6′,2″-terpyridine, Table 3)[44] complexes. Such an effect is masked in the crystal structure of **4**,[41] where the disorder of the Mn^{III} and Mn^{IV} ions leads to crystallographically equivalent Mn ions in the dimer. The assignment of **3** as a Mn(IV/IV/IV/IV) tetramer is, therefore, supported by the absence of Jahn−Teller effects and by the similarity between the Mn(1)−N and Mn(2)−N bond distances (Tables 2 and 3). In addition, the Mn−N distances of **3** are similar to the Mn^{IV}−N distances of **2**, **5**, **6**, and **7**, but they are shorter than those of Mn(III/IV)-disordered **4**, Mn^{III}−N of **6**, **7**, and *cis*-$[Mn^{III/III}_2O(terpy)_2(CF_3CO_2)_4]$ (*cis*-**8**)[43] (Table 3). The $N_{distal}-Mn-N_{distal}$ intraligand angles of **3** are also similar to those of **2** and **5** and larger than that of the distal-elongated Mn^{III} ions (Table 3). On the basis of these observations and the symmetry of the oxomanganese core, all four Mn ions of **3** are assigned as Mn^{IV}, all μ-O are assigned as μ-oxo groups, and the two terminal oxygen atoms on each of the distal Mn ions are assigned as a hydroxyl

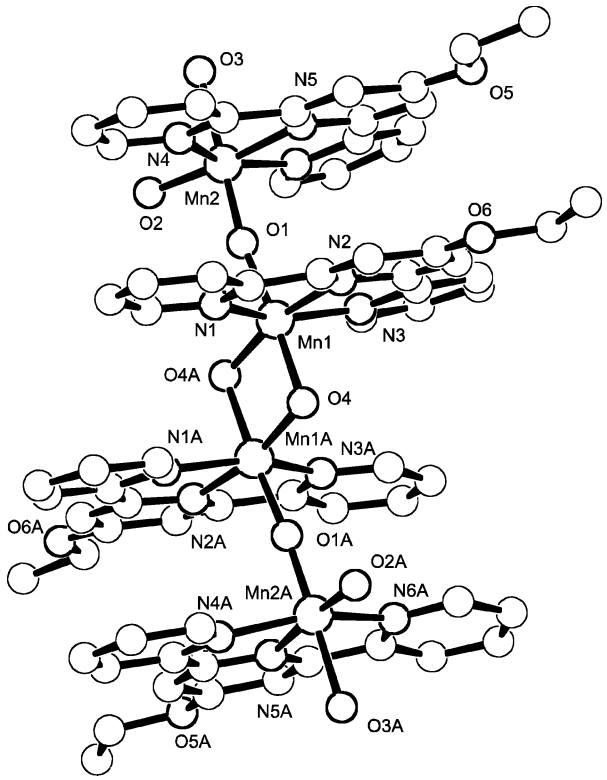

Figure 1. A drawing of the cation of **3** on the basis of its crystal structure, showing idealized spheres. Hydrogen atoms, perchlorate counterions, and waters of crystallization are omitted for clarity.

Table 2. Selected Bond Lengths (Å) and Angles (deg) for $\mathbf{3}\cdot 8H_2O$

Mn(1)−Mn(1A)	2.802(2)	Mn(1)−Mn(2)	3.506(1)
Mn(1)−O(1)	1.805(5)	Mn(2)−O(1)	1.714(5)
Mn(1)−O(4)	1.855(5)	Mn(2)−O(2)	1.833(5)
Mn(1)−O(4A)	1.807(4)	Mn(2)−O(3)	1.986(5)
Mn(1)−N(1)	2.040(6)	Mn(2)−N(4)	2.031(7)
Mn(1)−N(2)	1.993(6)	Mn(2)−N(5)	1.962(7)
Mn(1)−N(3)	2.035(6)	Mn(2)−N(6)	2.032(7)
Mn(1)−O(4)−Mn(1A)	99.8(2)	Mn(1)−O(1)−Mn(2)	170.1(3)
O(1)−Mn(1)−O(4).	174.6(2)	O(1)−Mn(2)−O(2)	94.2(2)
O(1)−Mn(1)−O(4A)	94.4(2)	O(1)−Mn(2)−O(3)	178.5(3)
O(1)−Mn(1)−N(1)	90.4(3)	O(1)−Mn(2)−N(4)	90.6(3)
O(1)−Mn(1)−N(2)	100.2(2)	O(1)−Mn(2)−N(5)	91.0(3)
O(1)−Mn(1)−N(3)	88.3(3)	O(1)−Mn(2)−N(6)	95.5(3)
O(4)−Mn(1)−O(4A)	80.2(2)	O(2)−Mn(2)−O(3)	85.7(2)
O(4)−Mn(1)−N(1)	90.2(2)	O(2)−Mn(2)−N(4)	101.2(3)
O(4)−Mn(1)−N(2)	85.2(2)	O(2)−Mn(2)−N(5)	174.8(3)
O(4)−Mn(1)−N(3)	93.3(3)	O(2)−Mn(2)−N(6)	100.5(3)
O(4A)−Mn(1)−N(1)	103.5(3)	O(3)−Mn(2)−N(4)	87.9(3)
O(4A)−Mn(1)−N(2)	165.3(2)	O(3)−Mn(2)−N(5)	89.1(3)
O(4A)−Mn(1)−N(3)	100.6(3)	O(3)−Mn(2)−N(6)	86.0(3)
N(1)−Mn(1)−N(2)	77.6(3)	N(4)−Mn(2)−N(5)	78.6(3)
N(1)−Mn(1)−N(3)	155.9(2)	N(4)−Mn(2)−N(6)	157.0(3)
N(2)−Mn(1)−N(3)	79.0(3)	N(5)−Mn(2)−N(6)	79.1(3)

(41) Limburg, J.; Vrettos, J. S.; Liable-Sands, L. M.; Rheingold, A. L.; Crabtree, R. H.; Brudvig, G. W. *Science* **1999**, *283*, 1524.
(42) Limburg, J.; Vrettos, J. S.; Chen, H. Y.; de Paula, J. C.; Crabtree, R. H.; Brudvig, G. W. *J. Am. Chem. Soc.* **2001**, *123*, 423.
(43) Baffert, C.; Collomb, M. N.; Deronzier, A.; Pecaut, J.; Limburg, J.; Crabtree, R. H.; Brudvig, G. W. *Inorg. Chem.* **2002**, *41*, 1404.
(44) Chen, H. Y.; Tagore, R.; Das, S.; Incarvito, I.; Faller, J. W.; Crabtree, R. H.; Brudvig, G. W. *Inorg. Chem.* **2005**, *44*, 7661.

Table 3. Selected Bond Lengths (Å) and Angles (deg) of High-Valent Polynuclear Mn−μ-Oxo Terpyridine Complexes[a]

	T (°C)	bond dist	$-N_d$	$-N_c$	$-N_d$	$-OH_2$	−mono-μ-O	$N_d-Mn^{III}-N_d$	$N_d-Mn^{IV}-N_d$
2[28]	−90	$Mn^{IV}{}_{av}-$	2.03	1.99	2.02	2.00	1.75		156.5
3	−90	$Mn^{IV}(1)-$	2.04	1.99	2.04		1.80		155.9
		$Mn^{IV}(2)-$	2.03	1.96	2.03	1.99	1.71		157.1
4[41 b]	−100	$Mn^{III/IV}-$[c]	2.10	2.04	2.10	2.01		150.5	150.5
5[42]	−90	$Mn^{IV}-$	2.01	1.99	2.04				155.5
6[43]	−80	$Mn^{III}-$[c]	2.26	2.13	2.27			143.9	
		$Mn^{IV}-$	2.03	2.00	2.02				155.6
7[44]	−90	$Mn^{III}-$[c]	2.19	2.05	2.22	2.00		148.4	
		$Mn^{IV}-$	2.04	2.04	2.06	1.99			153.8
cis-**8**[43]	−100	$Mn^{III}-$[c]	2.22	2.16	2.24		1.75	146.6	
trans-**8**[43 d]	0	$Mn^{III}{}_{av}-$[c]	2.09	1.99	2.08		1.75	156.6	

[a] **2**, $[Mn^{IV}{}_4O_5(terpy)_4(OH_2)_2](ClO_4)_6$; **3**, $[Mn^{IV}{}_4O_4(EtO\text{-}terpy)_4(OH)_2(OH_2)_2](ClO_4)_6$; **4**, $[Mn^{III,IV}{}_2O_2(terpy)_2(H_2O)_2](NO_3)_3$; **5**, $[Mn^{IV}{}_2O_2(terpy)_2(SO_4)_2]$; **6**, $[Mn^{III,IV}{}_2O_2(terpy)_2(CF_3CO_2)_2](ClO_4)$; **7**, $[Mn^{III,IV}{}_2O_2(mesityl\text{-}terpy)_2(H_2O)_2](NO_3)_3$; **8**, $[Mn^{III,III}{}_2O(terpy)_2(CF_3CO_2)_4]$; av, averaged; T, temperature of data collection; dist, distances; N_d, distal nitrogen; N_c, central nitrogen. [b]The Mn^{III} and Mn^{IV} ions are crystallographically equivalent (disordered). [c] Jahn−Teller distortion along the N_d-Mn-N_d axis. [d] Jahn−Teller elongation of the O−Mn−O axis along $CF_3CO_2^-$ ligands.

group and a water molecule. This assignment of the oxidation states is further supported by the magnetic susceptibility measurements (vide infra).

The three Mn−O bonds of the distal Mn ions have distinctively different distances of 1.99 (Mn(2)−O(3)), 1.83 (Mn(2)−O(2)), and 1.71 Å (Mn(2)−O(1)) and are, therefore, assigned as Mn−OH_2, Mn−OH, and Mn−oxo bonds, respectively (Tables 2 and 3). Indeed, as assigned, these Mn−O bond distances are close to those in relevant literature examples. The $Mn^{IV}-OH_2$ bond distances of **2**, **4**, and **7** are between 1.99 and 2.02 Å (Table 3); the Mn^{IV}−OH bond distances of $[Mn^{IV}{}_2O_2(tacn)_2(OH)_2]^{2+}$ and $[Mn^{IV}{}_3O_4(OH)(bpea)_3]^+$ are 1.88 Å[17] and 1.83 Å,[45] respectively, and the mono-μ-oxo−Mn^{IV} bond distances of **2**, *cis*-**8**, and *trans*-**8**[43] are 1.75 Å. It should be noted that in **3**, where the two mono-μ-oxo−Mn^{IV} bond distances are not equivalent, the trans effect of the oxo-bridged O(4) leads to a longer Mn(1)−O(1) distance (1.80 Å) compared to that of Mn(2)−O(1) (1.71 Å). Because of a similar trans effect of the mono-oxo bridge O(1), the di-μ-oxo bond distance of Mn(1)−O(4) (1.86 Å) is longer than that of Mn(1)−O(4A) (1.81 Å). Such trans effects have been shown in the literature to cause significant elongation of di-μ-oxo−Mn bond distances in **1** (1.74−1.91 Å)[26] and **2** (1.75−1.89 Å).[28] The O(3)−Mn(2)−O(1), Mn(2)−O(1)−Mn(1), and O(1)−Mn(1)−O(4) angles in **3** are 178.5, 170.1, and 174.6°, respectively, yielding a nearly linear conformation for O(3)−Mn(2)−O(1)−Mn(1)−O(4). The mono-μ-oxo bridge of **3** (Mn(2)−O(1)−Mn(1) 170.1°) is slightly more bent than that of **2** (178.6°), although the Mn−mono-μ-oxo−Mn distances (3.51 Å) are identical for both tetramers.

Compared with other tetranuclear manganese complexes (Scheme 1), the atom connectivity $Mn^{IV}(\mu\text{-}O)Mn^{IV}(\mu\text{-}O)_2$-$Mn^{IV}(\mu\text{-}O)Mn^{IV}$ in **3** leads to a particularly long distance between the terminal Mn atoms (Mn(2)···Mn(2A) 9.32 Å). This distance is much longer than those found in the two other linear tetramers **1** and **2**, 6.42 and 7.93 Å, respectively.

X-ray Powder Diffraction (XRD). Because of the similarity between the ligands, structure, and preparative methods of **2** and **3**, it is important to find out whether EtO-terpy could give a linear (2, 1, 2) tetranuclear oxo−manganese complex $[Mn^{IV}{}_4O_5(EtO\text{-}terpy)_4(OH_2)_2](ClO_4)_6$ (**3′**) that may have cocrystallized with the identified **3** (with a linear (1, 2, 1) core structure). Elemental analysis results cannot rule out structure **3′** because the difference of only one H_2O between **3** and **3′** is within the uncertainty of the data. The crystals of **3** appear to be uniform in shape under a microscope, and multiple crystallographic data collections on different crystals all yielded the same structure. These observations, however, are insufficient to prove the absence of **3′**.

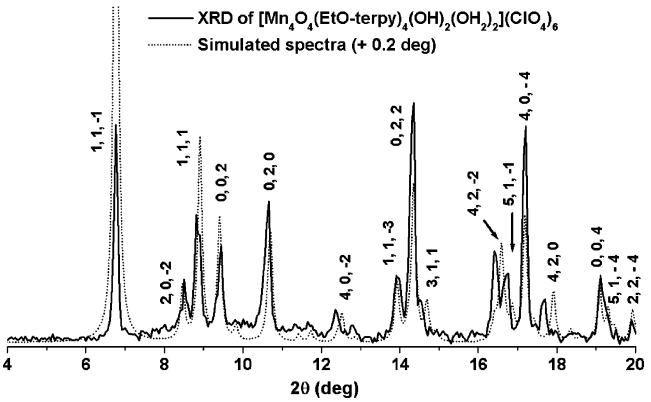

Figure 2. Powder XRD (solid line, collected at at $\lambda = 1.5405$ Å, $T =$ 25 °C) and simulated powder pattern of **3** (dotted line, simulated at $\lambda =$ 1.5405 on the basis of crystal structures collected at $\lambda = 0.71069$ Å, $T =$ − 90 °C). The indices (h, k, l) of the simulated peaks are presented in the figure.

XRD was, therefore, carried out on a bulk powder sample prepared from crystals of **3** to determine if the samples chosen for single-crystal X-ray diffraction were representative of the bulk sample. Figure 2 shows the XRD powder pattern of a bulk sample of **3** (collected at 25 °C), and the simulated XRD powder pattern based on the X-ray crystal structure of **3** (collected at −90 °C). The experimental and simulated spectra are analogous to each other, with only slight peak shifts at high 2θ angles, which may be the result of thermal expansion of the crystal cells at room temperature. Had the bulk sample of **3** contained **3′** as an impurity, the different symmetry and the different crystal cell dimensions of **3′** would be expected to result in a different set of diffraction peaks, in addition to those of **3**. The similarity between the experimental and simulated XRD powder patterns shows that the bulk sample contained only a single species, **3**; magnetic

(45) Pal, S.; Chan, M. K.; Armstrong, W. H. *J. Am. Chem. Soc.* **1992**, *114*, 6398.

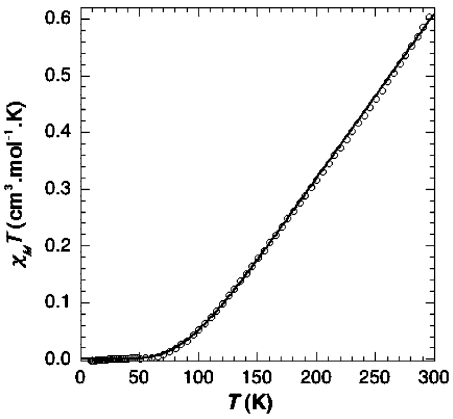

Figure 3. Plot of the product of the molar magnetic susceptibility and the temperature per mole of **3**·8H_2O vs temperature. The solid line corresponds to a fit (see text) with $J_1 = -432$ cm^{-1} and $J_2 = -164$ cm^{-1}.

susceptibility measurements are consistent with the absence of **3′** (vide infra).

Magnetic Properties. The variation of the molar magnetic susceptibility χ_M with temperature T has been investigated on a powder sample of **3**·8H_2O and is shown in Figure 3 as the $\chi_M T$ versus T plot. The $\chi_M T$ value measured at room temperature (0.603 cm^3 mol^{-1} K at 295.5 K) is far below the 7.5 cm^3 mol^{-1} K expected value for four uncoupled Mn^{IV} ions with electronic spins of $S_i = 3/2$ (i = 1, 1A, 2, 2A).

This indication of the strong antiferromagnetic exchange interactions in compound **3** was further confirmed by the decrease of the $\chi_M T$ product upon decreasing the temperature. A plateau at 0 cm^3 mol^{-1} K is reached below 55 K, indicating that **3** exhibits a well-stabilized diamagnetic ground state. The theoretical curve (solid line) shown in Figure 3 was obtained with $g = 1.98$, $J_1 = -432$ cm^{-1}, and $J_2 = -164$ cm^{-1}. It was equally possible to reproduce the experimental data with a g value ranging from 1.95 to 2.00. The terminal exchange constants, J_1, were assumed to be identical and varied from -422 to -440 cm^{-1}, while the central exchange constant, J_2, was between -154 and -171 cm^{-1}: the greater the g value, the more negative the J values. The large uncertainties on the J constants were surprising but can be easily understood by looking at the spin ladder. Regardless of the spin parameter set, the first excited spin state is a spin triplet that lies 279 ± 3 cm^{-1} above the diamagnetic ground state. The next excited spin states are the $S = 1$ and $S = 2$ levels that are $\sim$700 and $\sim$820 cm^{-1} above the $S = 0$ ground state, respectively. Consequently, the magnetic susceptibility of the tetranuclear species is mainly controlled by the separation between the singlet ground state and the first excited triplet state. These large energy gaps justify the absence of an X-band EPR signal (vide infra).

The terminal mono-μ-oxo pairs are more strongly antiferromagnetically coupled than the central di-μ-oxo unit. The J_2 value obtained from the di-μ-oxo pair is in agreement with the values determined for similar units present in polynuclear Mn^{IV}−oxo complexes: -152 cm^{-1} in $[Mn_3O_4(bpea)_3(OH)]^{3+}$,[45] -171 cm^{-1} in $[Mn_3O_4(bpy)_4(Cl)_2]^{2+}$,[46] and -176 cm^{-1} for the terminal di-μ-oxo pairs in **1**.[26,27] Strong antiferromagnetic exchange interactions ranging from -160 to -360 cm^{-1} were also found in dinuclear $[Mn^{IV}(\mu\text{-}O)_2Mn^{IV}]^{4+}$ core complexes synthesized with mixed oxygen/nitrogen ancillary ligands or fully nitrogen ones.[47] Law et al.[47] have shown that there is a correlation between the Mn−O−Mn angle and the exchange coupling for di-μ-oxo dimanganese complexes; the Mn−O−Mn angle (Mn(1)−O(4)−Mn(1A) = 99.8(2)°) and J value ($J_2 = -164$ cm^{-1}) determined here can be compared to the predicted value of -340 cm^{-1} (taking into account the different exchange Hamiltonians used in the two studies). Thus, the di-μ-oxo dimanganese unit in complex **3** is less antiferromagnetically coupled than expected on the basis of the published correlation. However, the correlation was based on magnetic data from dinuclear complexes, and complex **3** contains a dinuclear unit within a tetranuclear species. The two Mn^{IV} ions of the central di-μ-oxo dimanganese unit in complex **3** also have magnetic interactions with the terminal Mn^{IV} sites through mono-μ-oxo bridges. The di-μ-oxo dimanganese unit in complex **3** is, thus, not an isolated dinuclear compound, and this may explain why the correlation is not satisfied.

Mono-μ-oxo di-Mn^{IV} units are found in several tri- and tetranuclear complexes.[7] To our knowledge, there are only two unsupported mono-μ-oxo dinuclear Mn^{IV} complexes that have been characterized by X-ray diffraction, namely, the μ-oxo-bis[azido(tetraphenylporphinato)Mn^{IV}] complex[48,49] and the (μ-oxo)-bis[(cyclopentadienyl)(η^1-η^1-1,1,2,3,4,4-hexafluorobut-2-en-1,4-diyl)Mn^{IV}] species.[50] Only the room-temperature magnetic moment has been measured for the porphyrinato complex, and the observed 2.0 μ_B value suggests a strong antiferromagnetic interaction ($J \approx -300$ cm^{-1}). This is fully expected according to the linear geometry of the Mn−O−Mn core unit.[51] In tri- and tetranuclear complexes with the Mn_3O_4[45,46,52], the adamantane Mn_4O_6, or $Mn_4O_5(OH)$ cores,[18,53] the $Mn^{IV}(\mu\text{-}O)Mn^{IV}$ pairs are more bent, and the exchange interaction may be antiferromagnetic or ferromagnetic with coupling constants ranging from -108 cm^{-1} in $[Mn_3O_4(bpy)_4(Cl)_2]^{2+}$ [46] to 90 cm^{-1} in $[Mn_4O_6(bpea)_4]^{4+}$.[53] Compared with the couplings in these complexes, the terminal mono-μ-oxo di-manganese pairs of **3** are significantly more strongly antiferromagnetically coupled: $J_1 = -431 \pm 9$ cm^{-1}. A parallel can be drawn with the dinuclear $[LMn(\mu\text{-}O)MnL]^{2/3+}$ complexes containing a single unsupported mono-μ-oxo bridge within a $Mn^{III}Mn^{III}$ or a $Mn^{III}Mn^{IV}$ pair (L stands for the conjugated base of *N*,*N*-

(46) Auger, N.; Girerd, J. J.; Corbella, M.; Gleizes, A.; Zimmermann, J. L. *J. Am. Chem. Soc.* **1990**, *112*, 448.
(47) Law, N. A.; Kampf, J. W.; Pecoraro, V. L. *Inorg. Chim. Acta* **2000**, *297*, 252.
(48) Schardt, B. C.; Hollander, F. J.; Hill, C. L. *J. Chem. Soc., Chem. Commun.* **1981**, 765.
(49) Schardt, B. C.; Hollander, F. J.; Hill, C. L. *J. Am. Chem. Soc.* **1982**, *104*, 3964.
(50) Lentz, D.; Akkerman, F.; Kickbusch, R.; Patzschke, M. *Z. Anorg. Allg. Chem.* **2004**, *630*, 1363.
(51) Hotzelmann, R.; Wieghardt, K.; Florke, U.; Haupt, H. J.; Weatherburn, D. C.; Bonvoisin, J.; Blondin, G.; Girerd, J. J. *J. Am. Chem. Soc.* **1992**, *114*, 1681.
(52) Sarneski, J. E.; Thorp, H. H.; Brudvig, G. W.; Crabtree, R. H.; Schulte, G. K. *J. Am. Chem. Soc.* **1990**, *112*, 7255.
(53) Dube, C. E.; Sessoli, R.; Hendrich, M. P.; Gatteschi, D.; Armstrong, W. H. *J. Am. Chem. Soc.* **1999**, *121*, 3537.

bis(2-pyridylmethyl)-*N*′-salicyliden-1,2-diaminoethane).[54] These complexes exhibit comparably shorter Mn−O distances (1.727(2) Å for the Mn^{IV}−O bond length) and larger Mn−O−Mn bridging angles (178.7(2)° in the mixed valent species) to the ones measured in **3**. The two Mn ions are also strongly antiferromagnetically coupled: $J = -216$ and -353 cm^{-1} in the homovalent and mixed-valent complexes, respectively. The increasing antiferromagnetic interaction when going from the $Mn^{III}Mn^{III}$ to the $Mn^{III}Mn^{IV}$ species has been rationalized based on extended Hückel calculations.[54] Consequently, the even more negative J_1 constant for a $Mn^{IV}Mn^{IV}$ pair determined here is in perfect agreement with the previously observed behavior.

EPR Spectroscopy. X-band EPR spectra on a powder sample of **3** show no signal from 4 to 200 K. The lack of an EPR signal at helium temperature is consistent with a spin singlet ground state and, at higher temperature, with the large energy gap (279 cm^{-1}) between the first excited state and the diamagnetic ground state, as determined from the magnetic susceptibility data. In contrast, the much lower energy gap found in **1** (76.1 cm^{-1}) results in the appearance of an EPR signal for this compound at 40 K that reaches its maximal intensity at 130 K.[26,27]

Conclusion

A new type of high-valent Mn tetramer $[Mn^{IV}_4O_4(EtO\text{-}terpy)_4(OH)_2(OH_2)_2](ClO_4)_6$ has been synthesized and characterized by X-ray crystallography, XRD, EPR spectroscopy, and magnetic susceptibility studies. This compound contains an unprecedented linear (1, 2, 1) oxo-manganese core structure and is the first Mn^{IV} complex to be found to be coordinated by all three types of water-derived ligands, oxo, hydroxo, and aqua. Magnetic susceptibility studies have determined the exchange constants through the mono-μ-oxo and di-μ-oxo bridges to be -432 and -164 cm^{-1}, respectively. The large energy gap (279 cm^{-1}) between the $S = 0$ ground state and the first excited spin state is consistent with the absence of an EPR signal from this compound.

It is interesting that EtO-terpy yields complex **3** with a (1, 2, 1) oxo-manganese core structure, whereas terpy yields complex **2** with a (2, 1, 2) structure. At this time, it is not clear why the two ligands give different tetranuclear complexes. It is possible that the donation of electron density to the pyridyl ring by the ethoxy group helps to stabilize the (1, 2, 1) core structure which has fewer oxo ligands. There is also intermolecular hydrogen bonding in the crystal of **3** that is not present for **2**, which may stabilize the (1, 2, 1) structure. In addition, crystal-packing and π-stacking effects may be important.

Acknowledgment. The authors thank the National Institutes of Health (GM32715) and the US Department of Energy (DE-FG02-84E.R.13297) for financial support, Christopher Incarvito for assistance with the XRD measurements, Jean-Marc Latour of the Laboratoire de Physicochimie des Métaux en Biologie, UMR CEA CNRS 5046, CEA-Grenoble, France, for preliminary magnetic susceptibility measurements, and the Laboratoire d′Etude Dynamiques et Structurales de la Sélectivité, UMR CNRS 5616, Université Joseph Fourier, Grenoble, France, and the Département de Recherche Fondamentale sur la Matière Condensée, Service de Chimie Inorganique et Biologique, CEA-Grenoble, France, for access to EPR facilities.

Supporting Information Available: ORTEP drawing of **3**, x-ray crystallographic data of **3** (PDF), and the X-ray crystallographic file for **3** (CIF). This material is available free of charge via the Internet at http://pubs.acs.org.

IC051462M

(54) Horner, O.; Anxolabehere-Mallart, E.; Charlot, M. F.; Tchertanov, L.; Guilhem, J.; Mattioli, T. A.; Boussac, A.; Girerd, J. J. *Inorg. Chem.* **1999**, *38*, 1222.